Arch. Metall. Mater. **71** (2026), 2, 431-439

DOI: https://doi.org/10.24425/amm.2026.158822

SHANIBA PALAMADATHIL[1], ABDUL KAREEM THOTTOLI[2], SREELAKSHMI PUTHUMANA MELEPATTU[2], SHIVINA NANDHAYIL PARAMBIL[3], ATHIRA PRAKASH[4], MUHASIN MUBARAK K.P.[5], LABEEBA MANNISHERI[6], ISLAM M. AL-AKRAA[7], AHMAD M. MOHAMMAD[7], DEWI SURIYANI CHE HALIN[8], AYU WAZIRA AZHARI[9*]

ECO-DYING ON ZnO NANOPARTICLES USING TAMARINDUS INDICA L. SEED COAT TANNIN

This study aims to explore the potential of *Tamarindus indica L.* seed coat tannin as a natural dye sensitiser for zinc oxide nanoparticles. The tannin extract was prepared by mixing ground seeds with de-ionised water and utilised as a natural dye to sensitise ZnO nanoparticles, enhancing their optical absorption properties in the visible region. ZnO nanoparticles were synthesised in the presence of varying concentrations of Tamarindus indica L. seed coat tannin to investigate its impact on their growth and optical behaviour. Results demonstrated that the *Tamarindus indica* L. seed coat extract contained abundant polyphenolic compounds with characteristic hydroxyl groups, confirming its suitability as a natural sensitiser, while Fourier-transform infrared spectroscopy indicated strong chemical interactions between tannin molecules and zinc oxide through Zn–O bonding. Ultraviolet-visible analysis revealed that tannin incorporation extended the optical absorption edge of zinc oxide nanoparticles from 400 to 800 nanometres, shifting it into the visible spectrum. X-ray diffraction confirmed a hexagonal wurtzite structure with an average crystallite size of approximately 17 nanometres, supported by transmission electron microscopy observations. These findings demonstrate that *Tamarindus indica* L. seed coat tannin effectively enhances the light-harvesting capability of zinc oxide nanoparticles, offering a sustainable, low-cost approach for improving the optical performance of zinc oxide-based materials in dye-sensitised solar cells and other optoelectronic applications.

Keywords: Eco-dyeing; Tamarindus Indica L.; ZnO nanoparticles; dye-sensitised ZnO

1. Introduction

Nanotechnology focuses on materials with at least one dimension in the 1-100 nm range, often leading to unique and enhanced properties. Recent advancements in nanotechnology have emphasised the green synthesis of nanoparticles, aiming for sustainable and eco-friendly methods while reducing harmful byproducts [1]. Tamarindus indica L., the tamarind tree also known as Puli in South India, is one of the most common multipurpose tree species in the Indian sub-continent and is largely planted in South India. Many South Indian dishes are prepared with tamarind fruit pulp, which has also found places in the chemical and pharmaceutical industry. The brownish-red seed coat is about 30% of the seed, and the remaining is white kernel. The kernels are separated from the seed coat by roasting or soaking the seeds in water [2]. The antibacterial activity of the seed extract [3] and the polyphenolics present in the tamarind seed coat were dominated by proanthocyanidins [4].

Due to environmental pollution and health problems, the textile industry is moving to use natural dyes instead of synthetic dyes. In ancient times, Tamarindus indica L. seed coat tannin was used as a natural colourant, and it is anticipated that few villagers in South India still use it as a natural dark/brown colourant for their handmade clothes. Nowadays, without knowing the value of the seed, the hard brown part of the tamarind seed is left as waste in the food/chemical industry without using it as a colourant.

In one study, a multifunctional linen fabric was developed through a green in-situ synthesis of silver nanoparticles using

[1] GOVT. COLLEGE MALAPPURAM MUNDUPARAMBA, MALAPPURAM, KERALA 676509, INDIA
[2] DEPARTMENT OF PHYSICS, PSMO COLLEGE, TIRURANGADI, MALAPPURAM, KERALA, 676306, INDIA
[3] GRACE VALLEY COLLEGE OF ARTS AND SCIENCE, MARAVATTAM, MALAPPURAM, KERALA, INDIA
[4] KOTTAKKAL FAROOK ARTS AND SCIENCE COLLEGE, KOTTAKKAL, MALAPPURAM, KERALA, INDIA
[5] JAMIA NADWIYYA ARTS AND SCIENCE COLLEGE, EDAVANNA, MALAPPURAM, KERALA, INDIA
[6] DEPARTMENT OF CHEMICAL ENGINEERING, FACULTY OF ENGINEERING, THE BRITISH UNIVERSITY IN EGYPT, CAIRO 11837, EGYPT
[7] CAIRO UNIVERSITY, CHEMISTRY DEPARTMENT, FACULTY OF SCIENCE, CAIRO 12613, EGYPT
[8] UNIVERSITI MALAYSIA PERLIS, FACULTY OF CHEMICAL ENGINEERING AND TECHNOLOGY, 02600, PERLIS, MALAYSIA
[9] UNIVERSITI MALAYSIA PERLIS, FACULTY OF CIVIL ENGINEERING AND TECHNOLOGY, ENVIRONMENTAL ENGINEERING DEPARTMENT, 02600, PERLIS, MALAYSIA

* Corresponding author: ayuwazira@unimap.edu.my

tamarind seed coat extract [5], combined with a chitosan-based coating to enhance fabric properties. The modified linen demonstrated remarkable antibacterial activity, UV protection, flame retardancy, and antioxidant properties, effectively retaining these functions after 50 washes. This approach offers a sustainable route for producing textiles with enhanced functional properties suitable for various technical applications.

Further work with Tamarindus indica pulp extract enabled a one-step, sunlight-irradiated synthesis of ZnO/Ag nanostructures, which exhibited enhanced photocatalytic activity and significant antibacterial properties. These nanostructures were able to degrade toxic dyes like methylene blue and methylene orange efficiently, indicating their potential for environmental remediation and water purification. Moreover, their antibacterial activity suggests promising applications in biomedical fields, especially for antimicrobial coatings [6]. Another study involved an innovative approach that employed Tamarindus indica seed-shell nanoparticles combined with silver nanoparticles and Ceratonia silique locust bean gum fabricated a copper-micro mesh grid electrode for glucose detection. This biosensor displayed a high sensitivity and low detection limit for glucose, making it suitable for non-invasive glucose monitoring in artificial saliva. Such a platform has potential implications in point-of-care diagnostics, particularly for diabetic patients, underscoring the versatility of nanomaterials in healthcare applications [7].

A comprehensive review on plant-mediated green synthesis of metal nanoparticles highlights the use of diverse plant biomass for synthesising nanoparticles, which serve as sustainable and cost-effective alternatives to conventional synthesis methods. The review discusses their applications in environmental remediation, focusing on the degradation of toxic textile dyes in water. Factors such as pH, particle size, temperature, and radiation significantly affect nanoparticle formation and dye degradation efficiency, indicating the importance of synthesis conditions in optimising performance [8]. A recent study reported the synthesis of ZnO nanoparticles using tamarind bark extract in an alkaline medium, which effectively degraded textile dyes like methylene blue and Congo red. These ZnO nanoparticles showed promising antimicrobial properties, particularly against Gram-negative bacteria, supporting their application in water purification and wound healing. The study highlighted the catalytic and antimicrobial capabilities of ZnO nanoparticles, emphasising their utility in environmental and biomedical fields [9].

A concise review of zinc oxide nanoparticles (ZNPs) synthesised through biological methods revealed their high sensitivity, biocompatibility, and broad-spectrum antimicrobial activity. ZNPs have been investigated for applications in the animal industry as feed supplements, cancer treatment, drug delivery, bioimaging, and biosensing. The review also underscores the importance of understanding the toxicological effects of ZNPs on animals and the environment, calling for further research to optimise their safe usage across sectors [10]. These studies collectively emphasise the potential of green synthesis for developing functional nanomaterials. From environmental remediation and antimicrobial textiles to biosensing and biomedical applications, green-synthesised nanoparticles demonstrate remarkable utility across various domains. Future research should focus on large-scale synthesis, further toxicity assessments, and mechanism studies to enable broader commercial applications while ensuring environmental and biological safety.

Hence, this study utilised Tamarindus indica as a natural colourant in eco-dye to sensitise the ZnO nanoparticles. The findings of this work provide a new area of utilisation of large quantities of seed coats, which are available as residual material during the production of tamarind kernel powder and are used as a sizing agent. ZnO, an II-VI semiconductor nanomaterial, was chosen because of its unique characteristics over other metal oxide semiconductors, such as wide bandgap of 3.37 eV, large exciton binding energy (60 meV), high electron mobility, piezoelectric and pyroelectric properties, biocompatibility, non-toxic nature, very high specific surface area, good chemical and thermal stability [11]. ZnO nanoparticles are promising materials due to their unique, multifunctional properties that are suitable for creating photoanodes for dye-sensitive solar cells (DSSCs). In DSSCs, the photoexcitation of the dye molecules occurs when light is illuminated on the dye-sensitised ZnO layer, which subsequently injects electrons into the conduction band of the ZnO [12].

The main objective of this study is to discuss the potential use of the Tamarindus indica L. seed coat tannin to sensitise the ZnO nanoparticles and their characteristics. There are lots of reports available on green synthesis of ZnO nanoparticles using plant leaf, root, stem, flower and seed extracts, but no reports available on the synthesis of nanoparticles in Tamarindus indica L. seed coat tannin and of eco-dyeing of nanoparticles. Green synthesis of ZnO nanoparticles and eco-dyeing are different in the process itself. In the case of green synthesis, primarily based on plant extracts, the extracts are utilised to reduce and stabilise the nanoparticles. The phytochemicals in plant extracts can potentially reduce metal ions in a much shorter time than other reducing agents. The main phytochemicals present in plants are flavonoids, terpenoids, sugars, ketones, aldehydes, carboxylic acids, and amides, which are responsible for the bioreduction of nanoparticles [13]. However in the eco-dyeing process, natural dyes are used for surface modification and change their optical behaviour. The optical absorption and surface characteristics of eco-dyed ZnO nanoparticles are discussed here.

2. Methodology

Zinc acetate dihydrate ($Zn(CH_3COO)_2 \cdot 2H_2O$) and sodium hydroxide (NaOH) of 99.95% purity were purchased from Sigma-Aldrich Chemicals and used without further purification. De-ionised water was purchased from a local chemical supplier, and Fresh Tamarindus indica L seeds were collected directly from locally available plants. The collected Tamarindus indica L seeds were washed thoroughly using tap water followed by de-mineralised water. The seeds were roasted, and the brown peels were separated from the kernel seeds. The dried peels were crushed manually into a fine powder and stored for future use.

Various concentrations of Tamarindus indica L seed coat tannin were prepared by adding the prepared powder to 10 ml of de-ionised water under stirring. The mixture was stirred well using a magnetic pellet until it changed to a brownish-red-coloured solution. The extract was then filtered to remove the residues and impurities, and the brownish-red coloured filtrate was collected to use with ZnO nanoparticles. 20 ml of 0.75 M zinc acetate dihydrate was prepared in de-ionised water, then 10ml of the prepared Tamarindus indica L seed coat tannin solution of different concentrations was added slowly to the 0.75 M zinc acetate dihydrate solution under magnetic stirring. The mixture was stirred for 10 minutes by keeping the hotplate at 70°C. While stirring, 20 ml of 1 M NaOH solution was added dropwise to the mixture of zinc acetate dihydrate and tannin using a burette. A precipitate of ZnO was obtained, and the sodium acetate formed during the reaction process is soluble in water and can be removed by repeated washing. The supernatant was removed using a syringe, and the precipitate was washed many times using the syringe method. After repeated washing, the obtained precipitate was dried, and the resultant powder was collected for analysis.

X-ray diffraction (XRD) analysis of the powder samples was done at wavelength 0.1546 nm, running at 40 kV and 30 mA in an X-ray diffractometer (Bruker D8 Advance). X-ray diffractograms of zinc oxide nanoparticles were recorded in the region from 10o to 80o at a scan speed of 2o per minute. For UV spectroscopic analysis, prepared powder of ZnO nanoparticles was dispersed in distilled water (1 mg/ mL) and scanned in Agilent Cary 5000 UV–Vis spectrometer at 25°C in the range of 250-900 nm. Fourier Transform Infrared (FTIR) analysis of the ZnO was done by mixing ZnO nanoparticles and potassium bromide to form a salt plate. Spectra between 4000 and 400 cm^{-1} were recorded using a Thermo Nicolet Avtar 370 spectrometer.

3. Results and discussion

Tamarind seed coat tannin solution of various concentrations was prepared by mixing 0.2, 0.4, 0.6, 0.8, 1.0 and 1.2 mg of the prepared tamarind powder in 10 ml DI water to study the particle growth and absorption behaviour due to the dyeing effect. Tannins are made of polyphenolic compounds [1] and exist widely in plants. The extracts confirmed the presence of phenolic (–OH) groups [14], and the FTIR spectrum of the solution is shown in Fig. 1. Tsuda et al. [15] used ethanol and ethyl acetate as the extraction solvent and reported the isolation of phenolic compounds such as epicatechin, 2-hydroxyl 3',4'-dihydroxyacetophenone, methyl 3, 4-dihydroxybenzoate, and 3,4-dihydroxyphenyl acetate from the Tamarindus indica L seed coat tannin.

The FTIR spectra of the pristine ZnO nanoparticles and eco-dyed ZnO nanoparticles are shown in Fig. 2. The analysis was performed at room temperature in a frequency range of 4000-400 cm^{-1}. The observed peaks and corresponding vibrations are tabulated in TABLE 1 and TABLE 2 for liquid tannin and ZnO nanoparticles, respectively. The absorption intensity increases as the concentration of the tannin increases. When comparing the spectrum shown in Fig. 1 and Fig. 2, it can be seen that there are changes due to the attachment of ZnO with the tannin molecules. The spectrum also shows that the ZnO has attracted moisture from the surroundings. The spectrum presented a band at around 890 cm^{-1} and around 460 cm^{-1}, which signals

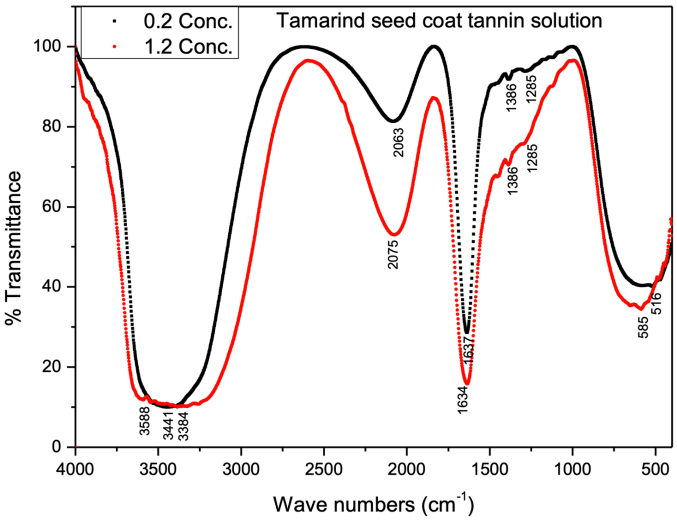

Fig. 1. FTIR Spectra of the Tamarindus indica L seed coat tannin solution

TABLE 1

FTIR bands and corresponding vibrations of *Tamarindus indica* L seed coat tannin solution [17]

Sample 0.2L	Sample 1.2L	Vibrations
3441	3588	OH stretching
3384	3384	OH stretching
2063	2075	C-C stretching vibration
1637	1634	C = C stretching vibration
1386	1386	CH_3 sym. bending
1285	1285	C-H sym. deformation vibration
516	585	C-C skeleton vibration

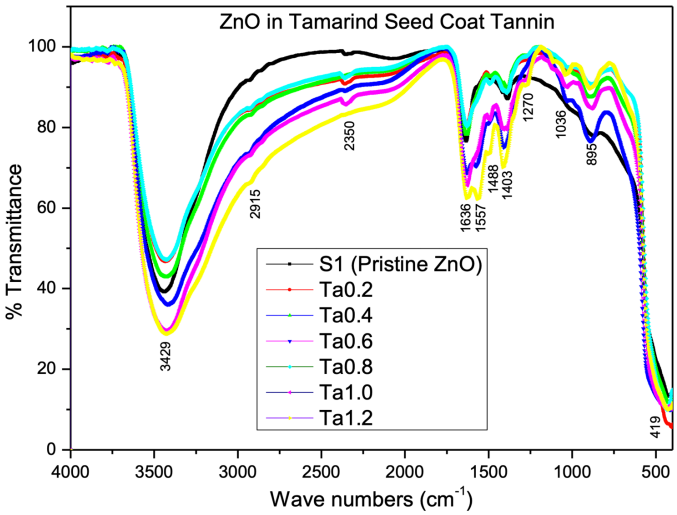

Fig. 2. FTIR Spectra of the eco-dyed ZnO using *Tamarindus indica* L seed coat tannin

TABLE 2

FTIR bands and corresponding vibrations of eco-dyed ZnO using *Tamarindus indica* L seed coat tannin [10]

S1	Ta0.2	Ta0.4	Ta0.6	Ta0.8	Ta1.0	Ta1.2	Vibrations
3439	3433	3430	3419	3425	3429	3421	OH Stretching
2915	2914	2915	2915	2915	2915	2915	–OH stretching vibration
2350	2350	2350	2350	2350	2350	2350	O–H stretching vibration
1633	1631	1632	1631	1631	1636	1626	O–H deformation vibration
—	1562	1559	1574	1550	1564	1557	Ring stretching or C=C stretching
—	1486	1454	1495	1455	1488	1499	H–O–H bending vibration mode due to the adsorption of moisture [18]
1386	1391	1389	1411	1393	1403	1412	hydrated zinc oxide [18]
—	1274	1272	1275	1272	1270	1278	O–H deformation and C–O stretching vibration interaction
—	1049	—	1033	1037	1036	1037	C–O stretching vibration
869	892	891	891	883	895	890	ZnO
424	403	428	461	—	419	422	ZnO stretching [18]

the characteristic bond of Zn–O and confirms the presence of zinc oxide in the sample.

The UV-visible absorption spectra of the prepared liquid samples at the concentrations of 0.2 and 1.2 (lowest and highest) were obtained as given in Fig. 3. It is observed that the tannin has absorption peaks around 300 nm (300 nm for 0.2 and 318 nm for 1.2), and two other absorption bumps were also observed for 1.2 at 375 and 570 nm and for 0.1 samples at 342 and 560 nm. In both samples, the absorption started from 700 nm and rose to 200 nm. Puksiri Sinchaiyakit et al. [16] reported a maximum absorption at around 280 nm for Tamarindus indica L seed coat tannin. The observed spectrum of our Tamarindus indica L seed coat tannin solution shows that the samples have absorption in the visible region, and the solution was reddish-brown. This absorption in the visible region helps us to sensitise ZnO nanoparticles to expand the ZnO spectrum to the visible region. In addition, the broadening of the absorption spectra is desirable for harvesting the solar spectrum in the visible region, leading to a higher photocurrent from the dye-sensitised solar cell.

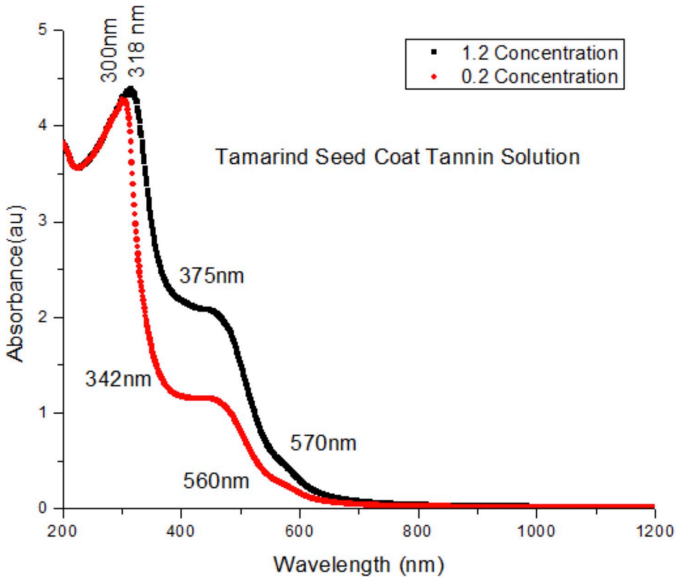

Fig. 3. Absorption spectra of the Tamarindus indica L seed coat tannin solution

The absorption spectra of the prepared ZnO nanoparticles powder were studied, as shown in Fig. 4. The absorption edge was observed at 390 nm (3.18 eV) for the pristine ZnO white powder. However, the absorption spectra of the ZnO prepared in the various concentrations of the tamarind tannin extended to the visible region (800 nm) with the same absorption bumps seen in the spectrum of the tannin solution alone. The absorption edge due to the ZnO in the eco-dyed sample has not moved remarkably from the position of the pristine sample. This means that the size of the ZnO has not changed much when prepared in the presence of tamarind seed coat tannin.

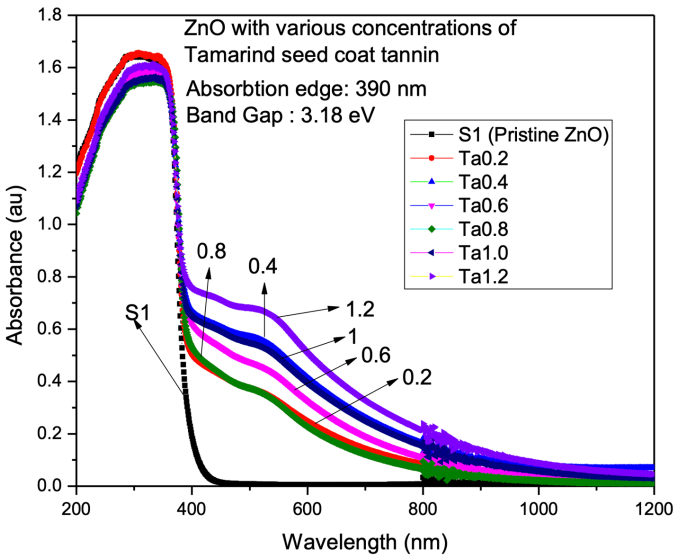

Fig. 4. Absorption spectra of the eco-dyed ZnO nanoparticles using Tamarindus indica L seed coat tannin

The bandgap of the prepared powder material was determined using the modified Tauc plot method proposed by Ragib Ahsan et al. [19]. For preparing the Tauc plot for nanoscale powders, Ragib Ahsan et al. [19] assumed that:

$$\frac{\Delta I}{I_o} = \alpha \Delta x \qquad (1)$$

From this equation, they derived as:

$$\frac{I_o}{I_T} = 1 + \alpha\Delta x \tag{2}$$

$$\alpha\Delta x = 10^A - 1 \tag{3}$$

$$\alpha \propto 10^A - 1 \tag{4}$$

Where A is the absorbance, α is the absorption coefficient, and I_o and I_T are the incident and transmitted photon intensity, respectively.

By using Eq. (4), the absorption coefficients (α) are calculated from the absorbance spectrum using the modified equation [19]. Here, the importance is given only to the linear part of the Tauc plot, and the value of absorption coefficients is approximated by considering that the absorption coefficient is proportional to the absorbance [19]. This alpha value is substituted in the Tauc plot Eq. (5) [20].

$$(\alpha h\nu)^{\frac{1}{n}} = A(h\nu - E_g) \tag{5}$$

Where h is plank's constant, ν is the photon frequency, α is the absorption coefficient, E_g the bandgap and A is the proportionality constant. The exponent's value denotes the electronic transition's nature, such as n = 1/2 for the direct allowed transition, n = 3/2 for the direct forbidden transition, n = 2 for the indirect allowed transition, and n = 3 for the indirect forbidden transition.

Generally, the allowed transitions dominate the basic absorption process, either n = 1/2 or n = 2, for direct and indirect transitions, respectively. Plotting and finding the best fit of the $(\alpha h\nu)^{\frac{1}{n}}$ vs $h\nu$ using n = 1/2 and n = 2 gives the correct transition type. The bandgap is found from the intersecting point of the curve in the energy axis. Here, the optical absorption strength is assumed to depend on the difference between the photon energy and the bandgap.

ZnO has a direct allowed transition [21] and draws the Tauc plot by substituting n = 1/2. At low energies, the photon energy absorption approached zero. At higher energies, the absorption process saturates, and the curve again deviates from linear, which is the characteristic of the Tauc Plot. At the rear of the bandgap, the absorption gets stronger and shows a region of linearity in the plot. This linear region is used to extrapolate to the x-axis intercept to find the band gap value.

The Tauc plots of the prepared powder samples are given in Fig. 5, and the band gaps found in the plots are presented in TABLE 3. It is observed that the bandgap has not shown many changes with the concentration of the tamarind seed coat tannin. This implies that the dye does not have any remarkable effect on controlling the particle size of the ZnO nanoparticles when ZnO nanoparticles are prepared using this method.

The UV-visible absorption spectra also give information about the Urbach tails related to the width of the localised states available in the optical bandgap of the ZnO nanoparticles. The band structure in the semiconductor may be damaged due to the disorder in the crystals or may be due to the addition of other extra atoms. Therefore, the Urbach energy found below the absorption band edge gives us an idea about the amount of damage to the crystal. For highly imperfect crystals, Urbach energy is large. The generation of absorption edge at the bandgap energy is due to the exciton phonon interaction or may be due to the electron-phonon interaction.

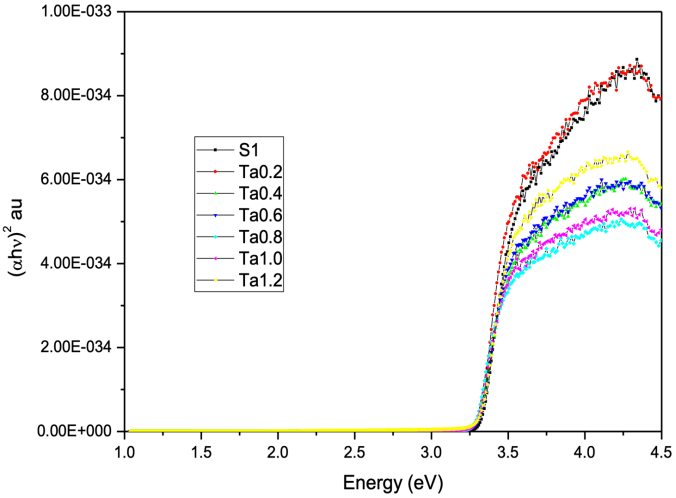

Fig. 5. Tauc plots of the prepared eco-dyed ZnO powder samples

TABLE 3

Band gap and Urbach energy of the eco-dyed ZnO

Sample	Band Gap (eV)	Slope from ln(α) vs $h\nu$ curve	Intercept	Urbach energy
S1	3.33	10.10142	–31.63335	0.0989
Ta0.2	3.32	10.68378	–32.99294	0.0935
Ta0.4	3.29	7.54507	–22.48141	0.1325
Ta0.6	3.30	10.63084	–32.84215	0.0940
Ta0.8	3.28	11.07669	–34.15198	0.0902
Ta1.0	3.28	10.08536	–30.92414	0.0991
Ta1.2	3.32	9.03697	–27.49977	0.1106

The defects in crystals also absorb light but do not contribute to free electrons; instead, they are recombined or trapped there. This is the curve in the Tauc plot after the absorption edge. Urbach energy gives the spectral dependence of the absorption coefficients examined at photon energies, which are less than the material's bandgap. That is the formation of localised states with energies at the boundaries of the energy gap, which is one of the effects of the structural disorder on the electronic structure of the material. These defect states trap the excited electrons and prevent the movement of an electron to the conduction band when the samples are irradiated with light of a particular wavelength. This absorption tail is called the Urbach tail and is associated with the Urbach energy. The equation for calculating the Urbach energy is

$$\alpha = \alpha_o + e^{\frac{h\nu}{E_u}} \tag{6}$$

Where α is the absorption coefficient, E_u is the Urbach Energy. The Urbach energy is calculated by plotting ln(α) vs $h\nu$. Fig. 6 shows the Urbach energy plots for all the samples. The slope and

intercept of the linear region were found using the linear quick-fit gadget tool in Origin Software. The reciprocal of the slope of the linear fit gives the Urbach energy values, and the Eu values are tabulated in TABLE 3 with bandgap energies. There are no significant changes in trend disorders as the tamarind seed coat tannin concentrations vary.

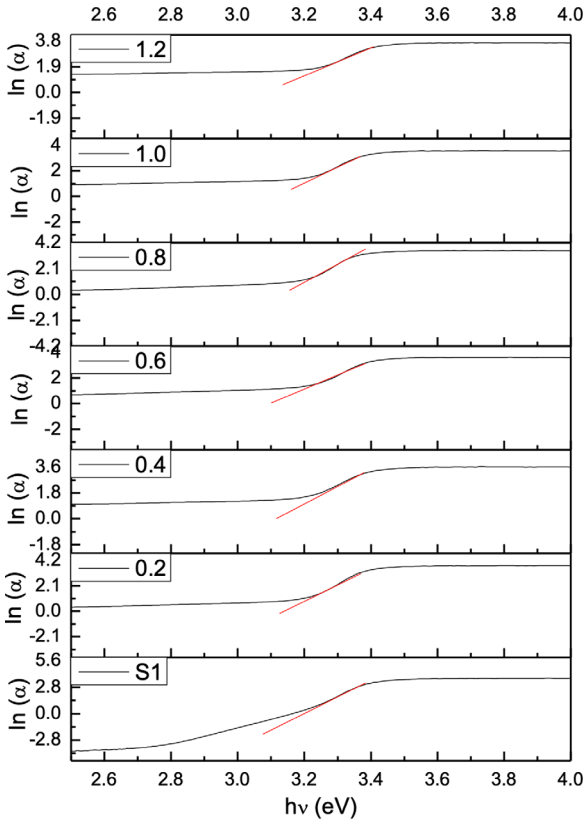

Fig. 6. Urbach energy curve for ZnO samples

XRD spectrum shown in Fig. 7 has prominent peaks corresponding to the diffraction peaks at 2θ = 31°, 34°, 36°, 47°, 56°, 62°, 65°, 67°, 72° and 76° were indexed with the diffraction planes (100), (002), (101), (102), (110), (103), (200), (112), (004) and (202) which well correlates with the JCPDS card no. 36–1451. The XRD pattern shows that the prepared ZnO has a hexagonal wurtzite structure (with a = b = 3.25 Å, c = 5.20 Å) belonging to the C46v space group (P63mc). The broadening of the peak in the XRD pattern clearly implies that small nanocrystals are present in the samples. There is no evidence of the bulk form of the materials and impurity. In the XRD pattern, the (101) diffraction peak is much stronger than other peaks. This indicates that the formed ZnO nanocrystals have a preferential crystallographic (101) orientation. The average crystallite size of the prepared sample was calculated using Debye-Scherrer's formula [22], i.e.,

$$D = \frac{0.9\lambda}{\beta \cos\theta} \tag{7}$$

where D is the particle size, λ the wavelength of x-rays (λ = 1.5406 Å for Cu Kα), θ the Bragg angle, and β is the full width at half maxima (FWHM). The average particle size (D) of synthesised ZnO nanoparticles was found to be 17 nm using this Eq. (7).

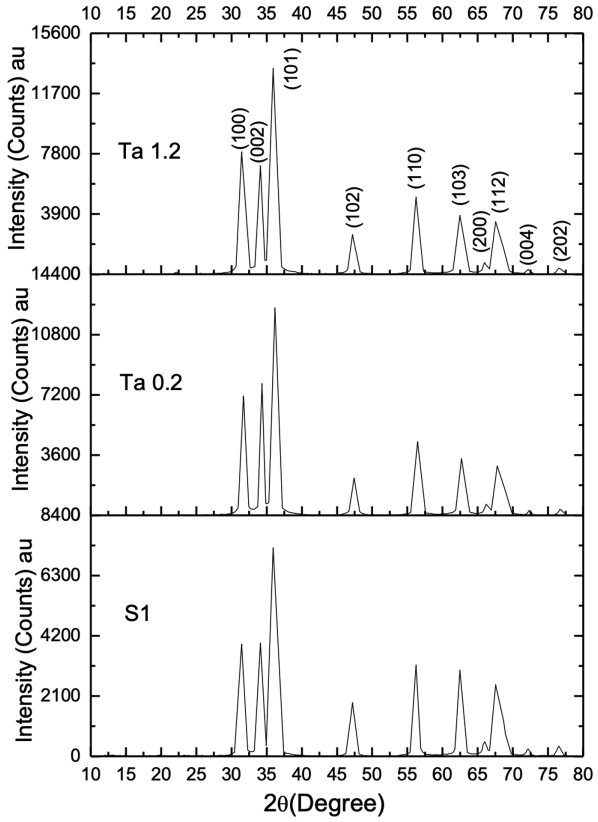

Fig. 7. XRD spectra of the prepared ZnO powder samples

The induced microstrain in the crystal due to the crystal imperfection and distortion was calculated using the equation [23]

$$\epsilon = \frac{\beta}{4\tan\theta} \tag{8}$$

The strain and particle size can also be found from the Williamson-Hall Plot. Williamson-Hall Plot was drawn using the equation

$$\beta \cos\theta = \frac{k\lambda}{D} + 4\ \epsilon \sin\theta \tag{9}$$

The plots were made by taking $4\sin\theta$ along the x-axis and $\beta\cos\theta$ along the y-axis for all the ZnO samples as shown in Figs. 8, 9 and 10. From the linear fit, the crystallite size was estimated from the y-intercept and the strain ϵ from the slope of the fit. [16] Geometric parameters of the prepared ZnO nanoparticles are tabulated for the samples S1, Ta0.2 and Ta1.2, as given in TABLES 4, 5 and 6. TABLE 7 shows the values obtained from Scherrer's formula and from the Williamson-Hall plot.

TEM and HRTEM images of the samples S1 and Ta0.2 are shown in Figs. 11 and 12. The images show that the particles are well separated in the nanoscale range. The interplanar spacing of 0.22 nm, as seen in Fig. 11, corresponds to the plane (101)

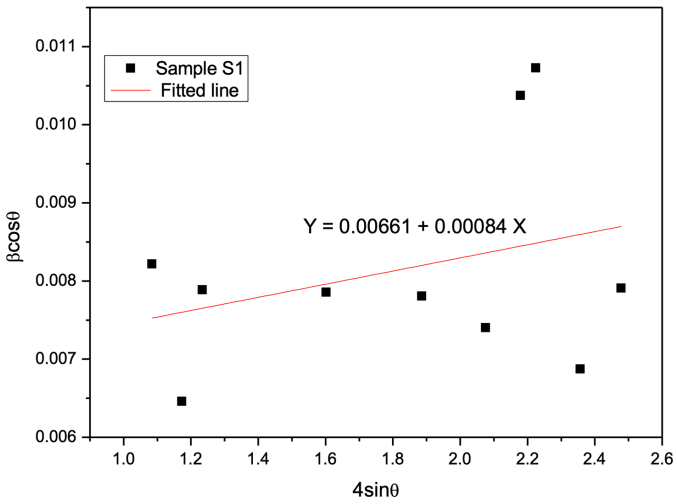

Fig. 8. Williamson-Hall plot pristine ZnO sample (S1)

TABLE 4

Geometric parameters of the ZnO nanoparticles of sample S1

2θ (degree)	Interplanar distance, d (Åm)	Standard JCPDS, d (Åm)	hkl	Crystallite Size, D (nm)	Micro strain, ϵ
31.43	2.84396	2.8143	100	16.9	0.007583
34.091	2.62785	2.6033	002	21.5	0.005507
35.921	2.49802	2.4759	101	17.6	0.006394
47.19	1.92444	1.9111	102	17.7	0.004905
56.225	1.63475	1.6247	110	17.8	0.004141
62.488	1.48511	1.4771	103	18.7	0.003567
65.992	1.41449	1.4071	200	13.4	0.004762
67.554	1.38552	1.3781	112	12.9	0.004822
72.158	1.30803	1.3017	004	20.2	0.002918
76.516	1.24402	1.2380	202	17.5	0.003192
Average				17.4	0.004779

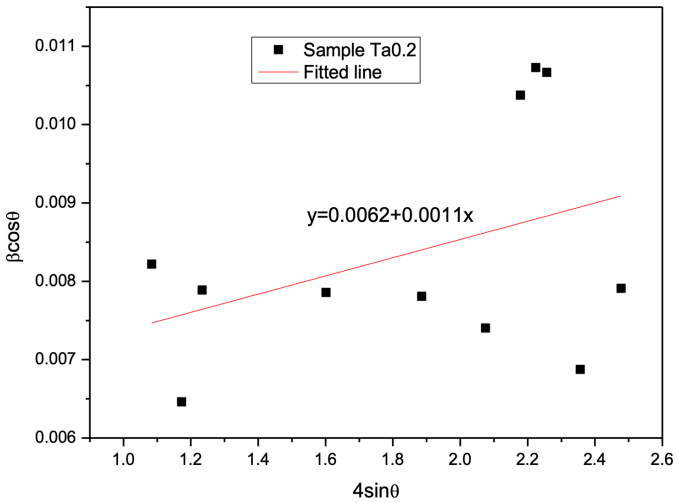

Fig. 9. Williamson-Hall plot pristine ZnO sample (Ta0.2)

TABLE 5

Geometric parameters of the ZnO nanoparticles of sample Ta0.2

2θ (degree)	Interplanar distance, d (Åm)	Standard JCPDS, d (Åm)	hkl	Crystallite Size, D (nm)	Micro strain, ϵ
31.43	2.84396	2.8143	100	16.9	0.007583
34.091	2.62785	2.6033	002	21.5	0.005507
35.921	2.49802	2.4759	101	17.6	0.006394
47.19	1.92444	1.9111	102	17.7	0.004905
56.225	1.63475	1.6247	110	17.8	0.004141
62.488	1.48511	1.4771	103	18.7	0.003567
65.992	1.41449	1.4071	200	13.4	0.004762
67.554	1.38552	1.3781	112	12.9	0.004822
72.158	1.30803	1.3017	004	20.2	0.002918
76.516	1.24402	1.2380	202	17.5	0.003192
Average				17.4	0.004774

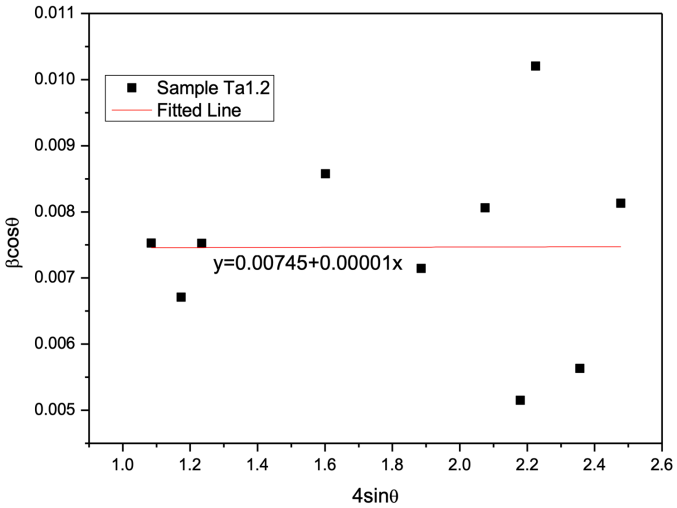

Fig. 10. Williamson-Hall plot pristine ZnO sample (Ta1.2)

TABLE 6

Geometric parameters of the ZnO nanoparticles of sample Ta1.2

2θ (degree)	Interplanar distance, d (Åm)	Standard JCPDS, d (Åm)	hkl	Crystallite Size, D (nm)	Micro strain, ϵ
31.457	2.84161	2.8143	100	18.4	0.006941
34.094	2.62759	2.6033	002	20.7	0.00572
35.931	2.4974	2.4759	101	18.4	0.006096
47.192	1.92437	1.9111	102	16.2	0.005354
56.238	1.63441	1.6247	110	19.4	0.003788
62.483	1.48522	1.4771	103	17.2	0.003884
66.006	1.41422	1.4071	200	26.9	0.002364
67.567	1.38539	1.3781	112	13.6	0.004586
72.165	1.30792	1.3017	004	24.6	0.00239
76.516	1.24401	1.2380	202	17.1	0.003281
Average				19.2	0.00444

plane, and the 0.24 nm in Fig. 12 also corresponds to the (101) plane. When comparing the tabulated values of XRD, it is seen that Tamarind seed coat tannin does not have much influence on their particle growth and size, as seen from the optical absorption studies and TEM analysis. However, their absorption properties are enhanced due to the eco-dyeing process.

TABLE 7

Crystallite size and microstrains of the samples S1, Ta02 and Ta1.2

Sample Name	Average Crystallite Size using Scherrer Formula (nm)	Average crystallite size from W-H plot	Micro strain from eqn.	Micro strain from W-H plot
S1	17.4	18.9	0.0047	0.00080
Ta0.2	17.4	20.1	0.0047	0.00110
Ta1.2	19.2	16.8	0.0044	0.00001

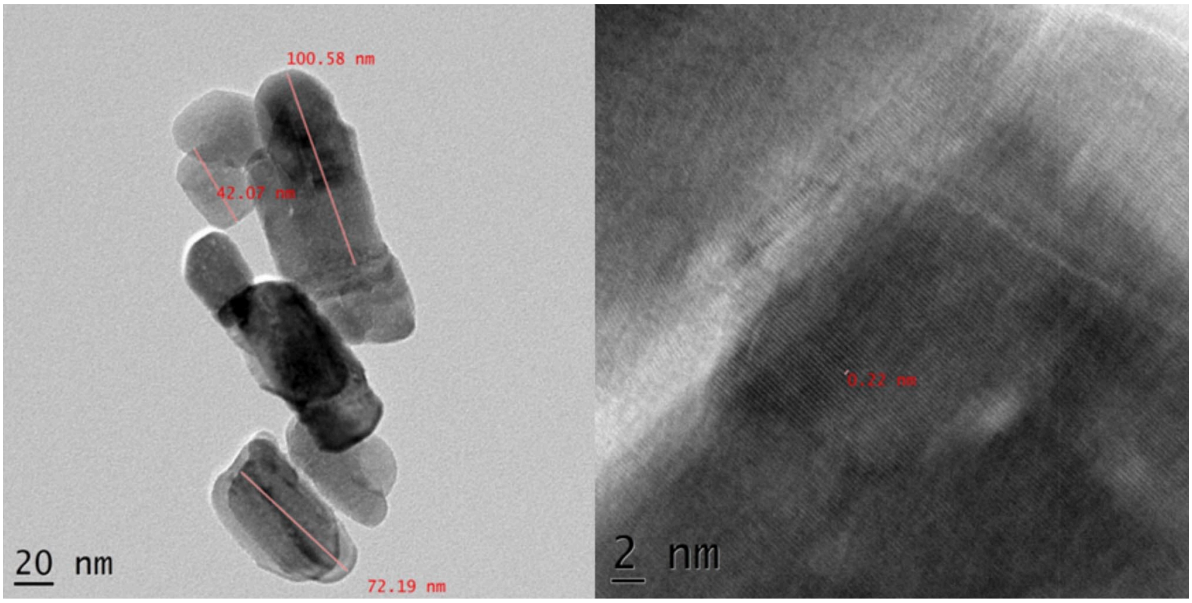

Fig. 11. TEM and HRTEM image of the Sample S1

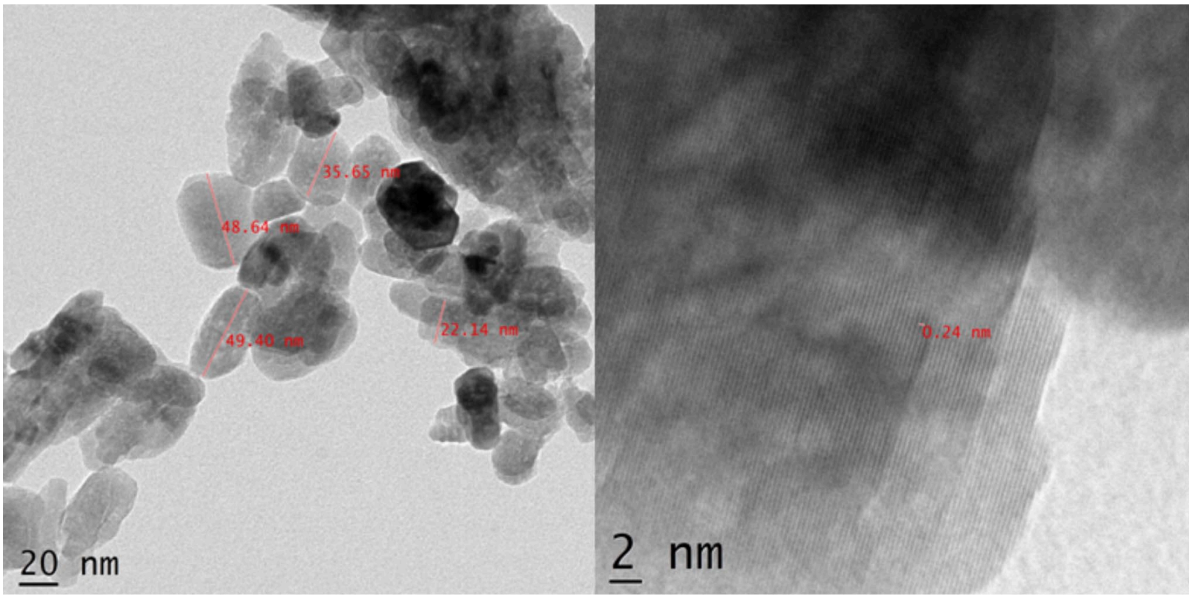

Fig. 12. TEM and HRTEM image of the Sample Ta0.2

4. Conclusion

Tamarindus Indica L. seed coat tannin was extracted, and their FTIR spectrum shows the presence of flavonoids, aldehydes and amides. The particle size of the prepared ZnO particles was calculated as approximately 17 nm. The UV-visible absorption spectroscopic results show that the optical behaviour is enhanced, and the eco-dyed ZnO can absorb a wide spectrum of light from 400 nm to 800 nm. Tamarind seed coat extract can be successfully employed as a natural dye to sensitise ZnO nanoparticles without changing their size.

Acknowledgements

We are highly indebted to P.O. Muneera, HOD, Department of Physics, M.K. Abdurahiman alias Bava and other Committee Members of Tirurangadi Orphanage and PSMO College for their invaluable support and encouragement.

REFERENCES

[1] Mrinalini Parmar, Mallika Sanyal, Extensive study on plant mediated green synthesis of metal nanoparticles and their application for degradation of cationic and anionic dyes. In Environmental Nanotechnology, Monitoring &Management. 100624 (2022).

[2] K.H. Prabhu, M.D. Teli, Eco-dyeing using Tamarindus indica L. seed coat tannin as a natural mordant for textiles with antibacterial activity. J. Saudi Chem. Soc. (2014).
DOI: https://doi.org/10.1016/j.jscs.2011.10.014

[3] M. De, A.K. De, A.B. Banerjee, Antimicrobial screening of some Indian spices. Phyther. Res. (1999). DOI: https://doi.org/10.1002/(SICI)1099-1573(199911)13:7<616::AID-PTR475>3.0.CO;2-V

[4] Y. Sudjaroen et al., Isolation and structure elucidation of phenolic antioxidants from Tamarind (Tamarindus indica L.) seeds and pericarp. Food Chem. Toxicol. (2005).
DOI: https://doi.org/10.1016/j.fct.2005.05.013

[5] Javed Sheikh, Indrajit Bramhecha, Multi-functionalisation of linen fabric using a combination of chitosan, silver nanoparticles and Tamarindus Indica L. seed coat extract. In Springer Nature (2019).

[6] Dayakar Thatikayala, Venkanna Banothu, Jinsub Park, Enhanced photocatalytic and antibacterial activity of ZnO/Ag nanostructure synthesised by Tamarindus indica pulp extract. Journal of Materials science: Materials in Electronics (2020).

[7] Dipali R. Bagal-Kestal, Been-Huang Chiang, Tamarindus indica seed-shell nanoparticles-silver nanoparticles-Ceratonia silique bean gum composite for copper-micro mesh grid electrode fabrication and its application for glucose detection in artificial salivary samples. International Journal of Biological Macromolecules (2021).

[8] Mrinalini Parmar, Mallika Sanyal, Extensive study on plant mediated green synthesis of metal nanoparticles and their application for degradation of cationic and anionic dyes. Environmental Nanotechnology, Monitoring & Management (2022).

[9] Baskar Gingiguntla, Abirami Akkiniraj Chandrasekar, Sebastian Antony Selvan Cruz, Green Mediated Synthesis of Zinc Oxide Nanoparticles using Tamarind Bark Extract and their Applications in Textile Dye Degradation and Antimicrobial Studies. Asian Journal of Chemistry (2023).

[10] Manoj Gadevar, G.K Prashanth and al., Unlocking nature's potential: Green synthesis of ZnO nanoparticles and their multifaceted applications – A concise overview. Journal of Saudi Chemical Society (2024).

[11] R. Kumar, A. Umar, G. Kumar, H.S. Nalwa, A. Kumar, M.S. Akhtar, Zinc oxide nanostructure-based dye-sensitised solar cells. Journal of Materials Science (2017).
DOI: https://doi.org/10.1007/s10853-016-0668-z

[12] C.S. Chou, F.C. Chou, Y.G. Ding, P. Wu, The effect of ZnO-coating on the performance of a dye-sensitised solar cell. Sol. Energy (2012). DOI: https://doi.org/10.1016/j.solener.2012.02.003

[13] J. Singh, T. Dutta, K.H. Kim, M. Rawat, P. Samddar, P. Kumar, 'Green' synthesis of metals and their oxide nanoparticles: Applications for environmental remediation. Journal of Nanobiotechnology (2018).
DOI: https://doi.org/10.1186/s12951-018-0408-4

[14] J. Coates, Interpretation of Infrared Spectra, A Practical Approach. In Encyclopedia of Analytical Chemistry (2006).

[15] T. Tsuda, M. Watanabe, K. Ohshima, A. Yamamoto, S. Kawakishi, T. Osawa, Antioxidative Components Isolated from the Seed of Tamarind (Tamarindus indica L.). J. Agric. Food Chem. (1994). DOI: https://doi.org/10.1021/jf00048a004

[16] P. Sinchaiyakit, Y. Ezure, S. Sriprang, S. Pongbangpho, N. Povichit, M. Suttajit, Tannins of tamarind seed husk: Preparation, structural characterisation, and antioxidant activities. Nat. Prod. Commun. (2011).
DOI: https://doi.org/10.1177/1934578x1100600619

[17] S. Thomas, Spectroscopic Tools. (2020). [Online]. Available: http://www.science-and-fun.de/tools/

[18] K. Handore et al., Novel green route of synthesis of ZnO nanoparticles by using natural biodegradable polymer and its application as a catalyst for oxidation of aldehydes. J. Macromol. Sci. Part A Pure Appl. Chem. (2014).
DOI: https://doi.org/10.1080/10601325.2014.967078

[19] R. Ahsan, M.Z.R. Khan, M.A. Basith, Determination of optical band gap of powder-form nanomaterials with improved accuracy. J. Nanophotonics (2017).
DOI: https://doi.org/10.1117/1.jnp.11.046016

[20] B.D. Viezbicke, S. Patel, B.E. Davis, D.P. Birnie, Evaluation of the Tauc method for optical absorption edge determination: ZnO thin films as a model system. Phys. Status Solidi Basic Res. (2015).
DOI: https://doi.org/10.1002/pssb.201552007

[21] A. Janotti, C.G. Van De Walle, Fundamentals of zinc oxide as a semiconductor. Reports Prog. Phys. (2009).
DOI: https://doi.org/10.1088/0034-4885/72/12/126501

[22] B.D. Cullity, Elements of X-ray diffraction, 2nd edition. Addison-Wesley Publ. Co. Read. MA (1978).

[23] T.A. Kareem, A. Kaliani, X-Ray Diffraction Study of Plasma Exposed and Annealed AlSb Bilayer Thin Film. Plasma Sci. Technol. (2013). DOI: https://doi.org/10.1088/1009-0630/15/4/13